Stem Cell Research & Therapy

RESEARCH

Open Access

Mesenchymal stem cells derived from hPSC via neural crest attenuate chemotherapy-induced premature ovarian insufficiency by ameliorating apoptosis and oxidative stress in granulosa cells

Xinran Li[1,2†], Jinrong Liao[1,3†], Youhong Zheng[1†], Wei Cai[1], Jie Chen[1], Yu Liang[1], Yuanmei Chen[1], Xiaoxuan Li[1], Jiamao Luo[1], Jiaxin Xie[1], Manping Zhou[1], Lilin Hang[1], Xiujuan Sun[1], Xin Yue[1], Xuefeng Wang[2*], Yifeng Wang[1*] and Huiyan Wang[1*]

Abstract

Background Premature ovarian insufficiency (POI) poses a significant threat to female reproductive health and currently lacks effective interventions. Recent studies highlight the promising potential of human pluripotent stem cell-derived mesenchymal stem cells (hPSC-MSC) in regenerative medicine. However, research on hPSC-MSC-based treatments for POI remains limited, particularly in the characterization of the intermediate differentiation stages from hPSC to MSC. This study presents an accelerated differentiation protocol for generating hPSC-MSC via neural crest cells (NCC) and evaluates their therapeutic potential in chemotherapy-induced POI.

Methods We modified a canonical small molecule-mediated protocol for hPSC-NCC-MSC differentiation. Systematic characterization of differentiated-cells was performed using qPCR, immunofluorescence, cell viability assays, flow cytometry and trilineage differentiation. In vivo, hPSC-NCC-MSC were transplanted into chemotherapy-induced POI SD rat models, and parameters such as body weight, ovarian weight, estrous cycle, hormone levels, follicle count, and mating were assessed. Granulosa cells (GC) apoptosis was analyzed using TUNEL assay and immunohistochemistry. In vitro, their effects on apoptosis inhibition and oxidative stress alleviation were investigated in a cultured GC cell line.

†Xinran Li, Jinrong Liao and Youhong Zheng contributed equally to this work.

*Correspondence:
Xuefeng Wang
15913130306@163.com
Yifeng Wang
wyf1988@163.com
Huiyan Wang
huiyanwang1990@163.com

Full list of author information is available at the end of the article

Additionally, comparisons between umbilical cord MSC (UC-MSC) and hPSC-NCC-MSC in chemotherapy-induced POI was conducted.

Results Our optimized protocol, combining CHIR99021 and SB431542, efficiently induced NCC from both human embryonic stem cells (hESC) and human induced pluripotent stem cells (hiPSC). The programmed hPSC-NCC-MSC, characterized by specific NCC markers (P75, HNK1, SOX10, and AP2α), exhibited typical MSC morphology, trilineage differentiation potential, favorable cell viability, and prominent anti-senescence properties. Among these, NCC differentiated from H1-hESCs (H1-NCC) demonstrated the highest induction efficiency (72.45%), and H1-NCC-derived MSC (H1-NCC-MSC) displayed superior proliferation and anti-senescence properties compared to UC-MSC. Besides, H1-NCC-MSC exhibited therapeutic efficacy comparable to UC-MSC in both in vivo and in vitro models of chemotherapy-induced POI, potentially through mechanisms involving reduced GC apoptosis, alleviated oxidative stress, and improved mitochondrial function.

Conclusions Our findings propose a modified hPSC-NCC-MSC differentiation protocol, offering an inexhaustible and stable source for regenerative therapies. Furthermore, we provide the first experimental evidence that hPSC-NCC-MSC have therapeutic potential comparable to UC-MSC in restoring chemotherapy-induced POI. The underlying mechanisms are likely associated with paracrine-mediated effects on GC apoptosis, oxidative stress, and mitochondrial dysfunction.

Keywords Human pluripotent stem cells, Neural crest cells, Mesenchymal stem cells, Premature ovarian insufficiency, Cyclophosphamide, Granulosa cells, Oxidative stress

Background

Premature ovarian insufficiency (POI) is a heterogeneous disorder characterized by the loss of ovarian function before the age of 40. It is marked by a reduction in ovarian follicles and elevated follicle-stimulating hormone (FSH) levels (>25 IU/L) [1]. POI patients often suffer from long term complications, including infertility, osteoporosis, cardiovascular diseases and depression, which pose significant threats to both the physical and mental health of women in reproductive age. Current clinical strategies fail to restore damaged ovarian function, highlighting the urgent need for effective therapies.

Mesenchymal stem cells (MSC) are a subset of adult stem cells with multipotent differentiation potential, high regenerative capacity, and strong immunomodulatory properties [2]. Umbilical cord-derived MSCs (UC-MSC), as a non-invasive source, have a higher proliferation rate than those derived from other adult tissues, offering a broad clinical application prospect in regenerative medicine. To date, over 150 trials involving UC-MSC have been registered on http://www.clinicaltrials.gov/. Multiple studies have shown that UC-MSC transplantation significantly elevates serum levels of hormones such as AMH and estradiol levels, while reducing follicular atresia, inhibiting granulosa cells (GC) apoptosis, and preventing ovarian fibrosis [3]. Despite their therapeutic potential, several drawbacks hinder the clinical translation of UC-MSC, including high heterogeneity obtained from different volunteers, limited proliferation capacity, compromised differentiation potential, and altered function in late passages [4, 5]. These challenges may explain the variability observed in preclinical studies of MSC efficacy. Thus, a new approach that ensures a stable and homogenous supply of MSC is critical for advancing POI cell therapy.

Human pluripotent stem cells (hPSC), such as human embryonic stem cells (hESC) and human induced pluripotent stem cells (hiPSC), have the capacity for indefinite proliferation and differentiation into all three germ layers [6]. This makes hPSC an attractive and accessible source for large-scale production of high-quality MSC [7]. However, the tumorigenicity of hPSC necessitates the development of reliable and efficient methods for generating specific cell types with clear and definite intermediate origins, ensuring their safety for therapeutic applications [8]. To address this issue, differentiation protocols involving neural crest cells (NCC) as intermediates have been established [9]. NCC belong to a transitional multipotent population that emerges during the development of embryonic ectoderm in vertebrates, making them a promising source for generating MSC [10]. Recent study has demonstrated that individual NCC differentiate into neurons and glia, forming dense innervation within the mouse ovarian medulla around E16.5 [11]. The migration of NCC-derived neurons and glia coincides with crucial patterning events in folliculogenesis, suggesting that neural innervation may facilitate primordial follicle formation [12] and the activation of the first wave of growing follicles after birth [13, 14]. In addition, innervations are located near the theca cell layer surrounding growing follicles [15], where they play a role in the activation of theca cells during follicle development and ovulation [16]. Therefore, the contribution of MSC derived from hPSC-NCC in POI cell therapy is of great interest.

In this study, we proposed a modified two-stage method to efficiently generate MSC from hPSC-derived

NCC (hPSC-NCC-MSC), which were characterized by MSC-specific markers, trilineage differentiation potential, robust proliferative capacity, and anti-senescence capacity. Among them, MSC derived from H1-hESC via NCC (H1-NCC-MSC) exhibited the highest proliferative rate. Subsequently, H1-NCC-MSC and UC-MSC were adopted to juxtapose their therapeutic effects on chemotherapy-induced POI models. In summary, our findings provide the first evidence that hPSC-NCC-MSC had favorable restorative ability in damaged ovaries, as indicated by the alleviation of GC apoptosis, oxidative stress and mitochondrial dysfunction. These results suggested that hPSC-NCC-MSC represent a novel and viable source of MSC for POI treatment.

Methods

Induction of neural crest cells (NCC) from human pluripotent stem cell (hPSC) lines

Two human embryonic stem cell (hESC) lines (H1, H9) and human embryonic fibroblasts-derived induced pluripotent stem cells (HEF-iPSC) were generously provided by Professor Xiafei Fu. The cells were cultured on Matrigel (Corning, USA)-coated plates using mTeSR medium (STEMCELL Technologies, Canada) supplemented with Y27632 (MedChemExpress, USA). The medium was refreshed daily, and the cells were passaged every 4–5 days using the StemPro Accutase Cell Dissociation Reagent (Life Technologies, USA).

For NCC induction, the culture medium was replaced with chemically defined medium (CDM) comprising Dulbecco's modified Eagle's medium/Ham's F-12 (DMEM/F12, KeyGEN, China) with 0.5 μM SB431542 (MedChemExpress, USA), and 1 or 3 μM CHIR99021 (MedChemExpress, USA). The medium was changed every 2 days from day 0 to 7. Cell morphology was monitored under an ECLIPSE Ti2 inverted microscope (Nikon, Japan). Specific markers for hESC (SOX2 and OCT4) and NCC (SOX10, AP2α and P75) were detected using qPCR. Additionally, P75, HNK1 and SOX10 expression was analyzed by flow cytometry (FCM) and immunofluorescence assays.

Differentiation of NCC to peripheral neuron cells

Briefly, $P75^{++}HNK1^{+}$ NCC on day 7 were sorted and seeded onto Matrigel-coated plates and cultured in Neurobasal medium (Gibco, USA) supplemented with B27 (Gibco, USA) and N-2 supplement (Gibco, USA), 2 mM L-glutamine (Gibco, USA), 10 ng/mL brain-derived neurotrophic factor (BDNF), glial cell line-derived neurotrophic factor (GDNF), 10 ng/ml nerve growth factor (NGF) and 10 ng/ml neurotrophin-3 (NT-3) (all from MedChemExpress, USA) for 3 weeks. The medium was replaced every 3 days. Differentiated peripheral neurons were identified by neural markers peripherin, β-Tubulin (TUJ1), tubulin beta 3 (TUBB3), S100 calcium binding protein (S100B) and glial fibrillary acidic protein (GFAP), as detected by immunocytochemistry.

hPSC-NCC expansion and phenotype maintenance

Induced cells were seeded onto Matrigel-coated plates and cultured in Neurobasal medium supplemented with B27 and N-2 supplement (N2B27), 20 ng/mL EGF, 20 ng/mL bFGF, 0.5 μM LDN-193189 (MedChemExpress, USA) and 3 μM CHIR99021. The medium was replaced every 3 days. hPSC-NCC were expanded to passage 3, at which point they were obtained for MSC differentiation.

Derivation of MSC from hPSC-NCC

The medium was replaced with DMEM/F12 containing 20% Fetal Bovine Serum (FBS, Excell, China), 55 μM β-mercaptoethanol (Gibco, USA), 2 mM L-glutamine (Gibco, USA), 1× MEM Non-Essential Amino Acids Solution (MEM NEAA, Gibco, USA), and Penicillin/Streptomycin. Changes in cell morphology were observed approximately 4 days after induction, and MSC identification was performed on day 12.

Isolation of umbilical cord mesenchymal stem cells (UC-MSC)

UC-MSC were obtained from parturient women who tested negative for infectious diseases, with written and informed consent provided for the use of umbilical cord sample for research purposes. Briefly, umbilical cords were washed and broken into small sections, then the blood vessels were removed. Umbilical cord sections were further cut into pieces (1 mm^3), then the pieces were transferred onto Matrigel-coated culture flask and cultured in the same medium as hPSC-NCC-MSC. The plates were kept at 37°C in a 5% CO_2 humidified atmosphere. After reaching approximately 80% confluence, UC-MSC were passaged. UC-MSC at passage 3–6 were utilized for subsequent experiments.

Characterization of UC-MSC and hPSC-NCC-MSC

MSC markers (CD29, CD44, CD73, CD90, CD105) and hematopoietic stem cells markers (CD34, CD45) were analyzed by Flow cytometry [28]. Trilineage differentiation was assessed by staining with Alizarin Red, Oil Red O and Toluidine Blue (Oricell, China) to identify osteoblast-like cells, adipocytes and chondrocytes, respectively. All procedures were performed according to the manufacturer's protocols.

Flow cytometry (FCM) and fluorescence activated cell sorting (FACS)

Cells were incubated with antibodies in FACS buffer (1% BSA in PBS) for 30 min at 4°C. All antibodies are listed in Supplementary Table 1. In each experiment, the

isotype-antibody served as a negative control. Following incubation, cells were washed with FACS buffer twice and resuspended. Subsequently, the cell suspension was passed through a 40 μm filter (Falcon, USA) and analyzed by CytoFLEX S Flow cytometry (BECKMAN COULTER, USA).

Immunocytochemistry (ICC)

Cells were fixed with 4% PFA at room temperature for 15 min, permeabilized with 0.3% TritonX-100 at 4 °C for 30 min, and incubated with primary antibodies at 4 °C overnight. Subsequently, cells were incubated with secondary antibodies in 3% BSA/PBS at 4 °C for 1 h. Nuclei were counterstained with DAPI for 10 min. Primary and secondary antibodies were listed in Supplementary Table 1. Observations were performed using ECLIPSE Ti2 inverted microscope (Nikon, Japan).

Senescence-Associated β-galactosidase (SA-β-Gal)

SA-β-Gal activity was detected using the SA-β-Gal kit (Beyotime, China). MSC were fixed at room temperature for 15 min and subsequently stained with 1 mL of working solution then were incubated at 37 °C overnight. The optical microscope (Nikon, Japan) was used for the subsequent observation of senescent cells.

Animals

7-week-old female and male wild type Sprague-Dawley (SD) rats were purchased from BesTest Biotechnology Co., Ltd. (China). Rats were housed in 22 °C ± 2 °C environment with a 12-hour light/dark cycle, provided with ad libitum access to water and food. After a two-week acclimatization period, SD rats with stable estrous cycles ($n = 28$) were selected for the study. All experimental procedures were approved by Experimental Animal Center at Southern Medical University and granted approval by the Ethics Committee of the Experimental Animal Center at Zhujiang Hospital (LAEC-2022-170). The work has been reported in line with the ARRIVE guidelines 2.0.

Premature ovarian insufficiency (POI) rat model establishment and MSC transplantation

SD rats ($n = 28$) were randomly assigned to 4 groups: control, POI, UC-MSC and H1-NCC-MSC. Random assignment to groups was performed using the "Random Number Generator" function in SPSS software. Rats in the latter 3 groups received an intraperitoneal loading dose of cyclophosphamide (CTX; 50 mg/kg, Sigma-Aldrich, USA), followed by daily intraperitoneal injections of 8 mg/kg for 14 consecutive days. Rats in control group were administered an equivalent volume of DPBS instead. In the UC-MSC and H1-NCC-MSC groups, 1×10^6 DiD-labelled (KeyGEN, China) UC-MSC or H1-NCC-MSC in 100 μL DPBS was injected into the tail vein 24 h after the final CTX dose. In the control and POI groups, 100 μL of DPBS alone was injected. MSC transplantation was repeated weekly for two additional weeks [17]. All rats were continuously monitored for estrous cycles throughout the experiment and sacrificed ($n = 3$ in each group) or mated ($n = 4$ in each group) one week after the final MSC injection. At the experimental endpoint, intraperitoneal anesthesia was administered using a 2% working solution of 2,2,2-tribromoethanol and tert-amyl alcohol (all from Sigma-Aldrich) at a dose of 400 mg/kg. After the entered unconsciousness, euthanasia was performed by exsanguination via the abdominal aorta.

Fertility assessment

The mating trials lasted for 1 month and litter size in each group ($n = 4$) was recorded.

H&E staining

Ovaries were collected and fixed in 4% PFA for paraffin embedding and sectioning. Serial Sections (5 μm thick) were obtained, and every fifth section was stained with hematoxylin and eosin for follicle counting. Based on previous references, ovarian follicles were classified as primordial, primary, secondary, or antral [18].

Terminal-deoxynucleotidyl transferase mediated nick end labeling (TUNEL) Deparaffinized tissue sections were permeabilized with 20 μg/mL DNase-free proteinase K for 20 min at 37 °C. The sections were incubated with 50 μL TUNEL reaction solution for 1 h at 37 °C in the dark, followed by treatment with 50 μL of Streptavidin-HRP fluorescein reagent for 30 min at 37 °C. Nuclei were counterstained with DAPI. TUNEL-positive cells in the ovary staining green and were observed under ECLIPSE Ti2 inverted microscope.

Immunohistochemistry (IHC)

Paraffin sections were dewaxed, rehydrated, and treated to block endogenous peroxidase activity by incubation in 3% hydrogen peroxide in methanol for 15 min. Antigen retrieval was performed in 10% trisodium citrate. After blocking with goat serum (Boster, China) for 1 h, the sections were incubated overnight at 4 °C with primary antibodies (listed in Supplementary Table 1). On the following day, diaminobenzidine (DAB) reagent was applied for coloration. Non-immune immunoglobulin G (IgG) was used as a negative control.

Immunofluorescence (IF)

To track the transplanted DiD-labeled MSC in vivo, ovaries from each group were fixed in 4% PFA for 24 h, followed by 20% and 30% sucrose gradient dehydration, and embedded in OCT. Serial Sect. (10 μm thick) were prepared, washed with PBS and counterstained with DAPI

at room temperature for 5 min. Observations were conducted using an ECLIPSE Ti2 inverted microscope.

Enzyme-Linked immunosorbent assay (ELISA)

Whole blood samples collected in heparin were centrifuged at 3,000 rpm for 20 min. Plasma was collected and stored at -80 °C. Cell culture medium was centrifuged at 1,500 rpm for 10 min to remove the cell and debris. E_2 (R&D system, USA), FSH (NEWA, China) and AMH (NEWA, China) levels were measured by ELISA kit according to the manufacturer's instructions.

Safety assessment of hPSC-NCC-MSC and UC-MSC

Histological evaluation of the heart, liver, kidney, lung, and spleen was performed using H&E staining on rat tissues after H1-NCC-MSC and UC-MSC transplantation. Serum levels of alanine aminotransferase (ALT), aspartate aminotransferase (AST), creatinine (Cr), and lactate dehydrogenase (LDH) were measured using commercial detection kits (NJJC Bio, China).

Preparation of MSC-conditioned medium (MSC-CM)

In brief, after washed several times with PBS, the medium of MSC was replaced with serum-free DMEM-F12 then maintained in incubator for 48 h, after which CM were collected and centrifuged at 1500 rpm for 10 min to remove cell debris or detached cells. The CM was then filtered through a 0.22 μm filter and stored at -80 °C.

KGN cell line and in vitro experiment design

KGN cell line was purchased from HyCyte (TCH-C230) to investigate whether MSC exert protective effects on chemotherapy-damaged GC in vitro. An in vitro model was established using 4-hydroperoxy cyclophosphamide (4-HC) [19], an active cyclophosphamide metabolite. KGN cells were separated into four groups, including NC, 4-HC, 4-HC + UC-MSC-CM and 4-HC + H1-MSC-CM. Cells in the NC group received no intervention, while cells in the remaining groups were pre-treated with 4-HC (15 μM) for 48 h. In the treatment groups, 4-HC was replaced with MSC-CM supplemented with 10% FBS, and cultures were maintained for an additional 48 h. KGN cells with indicated interventions were collected for in vitro experiments.

Cell counting Kit-8 (CCK-8) assay

KGN cells (5×10^3 cells/well) with indicated treatments were seeded into 96-well plates. A total of 10 μL of CCK-8 solution (Glpbio, USA) was added to each well, and cells were incubated at 37 °C for 2 h. Absorbance at 450 nm was measured using a microplate reader (BioTek, USA). All experiments were performed in triplicate.

Annexin V-FITC/PI apoptosis assay

The FITC Annexin V-FITC/PI Apoptosis Kit (Elabscience, China) was used to assess apoptosis in KGN cells. After washing, cells were resuspended in 500 μL of 1× binding buffer and mixed with 5 μL of Annexin-V-FITC and 5 μL of propidium iodide (PI). The fluorescence intensity was analyzed by flow cytometry (FCM). Experiments were repeated in triplicate.

Reactive oxygen species (ROS) detection

For intracellular ROS detection, KGN cells in a six-well plate were incubated with 10 μM DCFH-DA (Beyotime, China) at 37 °C for 20 min. After washing and resuspension in 100 μL of PBS, ROS fluorescence intensity was analyzed by FCM.

For mitochondrial ROS detection, cells were stained with 5 μM MitoSOX Red at 37 °C for 30 min, followed by Hoechst 33,342 counterstaining for 10 min. Fluorescence was visualized using a fluorescence microscope and quantified by FCM.

Mitochondrial membrane potential assay kit with JC-1

The JC-1 Mitochondrial Membrane Potential Assay Kit (Solarbio, China) was used to assess mitochondrial membrane potential changes. Cells were incubated with 5 μM JC-1 fluorescent dye for 30 min, washed twice with PBS, and visualized under a fluorescence microscope. Green fluorescence indicated membrane depolarization and mitochondrial damage, while red fluorescence represented intact mitochondria.

MDA, SOD and GSH detection

Commercial kits (MDA: Solarbio, China; SOD and GSH: Beyotime, China) were used to measure malondialdehyde (MDA), superoxide dismutase (SOD), and glutathione (GSH) levels, respectively. KGN cells (1×10^6 cells) were washed three times with PBS and lysed for 10 min. Lysates were centrifuged at 12,000 rpm for 15 min at 4 °C, and supernatants were collected to measure protein concentrations and perform assays according to the manufacturer's instructions.

Quantitative RT-PCR (qPCR)

Total RNA was extracted from ovaries and cells using TRIzol reagent. RNA (1,000 ng) was reverse-transcribed into cDNA using Evo M-MLV RT Premix for qPCR. Quantitative PCR was conducted using SYBR Green Premix Pro Taq HS qPCR Kit (Accurate Biology, China) and a Real-Time PCR System (Bio-Rad, USA). Relative gene expression was calculated using the ΔCt method, normalized to GAPDH and β-actin. Primer sequences are listed in Supplementary Table 2.

Western blotting

Ovarian tissues were lysed using RIPA buffer containing protease and phosphatase inhibitors. Protein concentrations were normalized using a BCA assay, and samples were subjected to SDS-PAGE electrophoresis. Antibodies used are listed in Supplementary Table 1.

Statistical analysis

All data are presented as the mean ± SD. Comparisons between groups were performed using a one-way ANOVA analysis. $p < 0.05$ was considered statistically significant. All statistical analyses were performed using Graphpad Prism 9.0 (R&D scientific software, USA).

Results

Differentiation and characterization of human pluripotent stem cells-derived neural crest cells (hPSC-NCC)

To optimize differentiation conditions, two regimens were evaluated for their efficacy in directing hPSC toward NCC (Fig. 1A). H1-hESC, H9-hESC, and HEF-iPSC were used in this study, with the main text presenting data for H1-hESC. Over time, the majority of cells in the NCN2-1 group and a small proportion in the NCN2-2 group transitioned from colony morphology to a stellate-like appearance (Fig. 1B). By day 7, 72.45% of cells in the NCN2-1 group and 1.79% in the NCN2-2 group were $P75^{++}/HNK1^{+}$ positive, indicating a higher induction efficiency in the NCN2-1 group (Fig. 1C). As differentiation progressed, the mRNA expression of NCC markers (P75, HNK1, SOX10, and AP2α) in the NCN2-1 group was significantly upregulated, while the expression of pluripotency markers (OCT4 and SOX2) was rapidly downregulated (Fig. 1D). This trend was further confirmed by fluorescent immunocytochemistry for SOX10 (Fig. 1E). These results indicated that the NCN2-1 regimen, which included 1 μM CHIR99021 and 0.5 μM SB431542, was more effective and was selected for subsequent experiments.

To confirm that the differentiated cells exhibited hPSC-NCC characteristics, $P75^{++}/HNK1^{+}$ cells were enriched by FACS and found to co-express SOX10 and AP2α (Fig. 1F-H). Moreover, these cells successfully differentiated into peripheral neurons under directed conditions, demonstrating functional NCC properties (Fig. 1I; Figure S1). Using the NCN2-1 regimen, H9-hESC and HEF-iPSC were also differentiated into NCC, as confirmed by morphology, immunostaining, and flow cytometry (Figure S2A-D).

Differentiation of mesenchymal stem cells derived from hPSC-NCC (hPSC-NCC-MSC)

The culture medium was optimized to preserve the characteristics of expanded hPSC-NCC (Fig. 2A). Briefly, sorted $P75^{++}/HNK1^{+}$ hPSC-NCC were cultured in N2B27 medium with or without LDN-193189 and CHIR99021 (LC), and NCC markers were assessed at passage 3 and 6. Cells maintained their morphology in the N2B27 + LC group, which also exhibited relatively high mRNA levels of P75, HNK1, SOX10 and AP2α compared to the N2B27 group at passage 6 (Fig. 2B-C). These findings indicated that N2B27 + LC was the optimal culture medium for maintaining the hPSC-NCC phenotype.

To obtain MSC from hPSC-derived NCC, the NCC maintenance medium was replaced with MSC-induction medium (Fig. 2D). By 20 days of induction, cells displayed the fibroblast-like morphology characteristic of MSC, a feature that became more pronounced with passaging (Fig. 2E). hPSC-NCC-derived MSC (hPSC-NCC-MSC) were harvested at passage 4 for further characterization.

Identification and characterization of hPSC-NCC-MSC

Over 98% of hPSC-NCC-MSC expressed the MSC markers CD29, CD73, CD44, CD90, and CD105, while lacking the hematopoietic markers CD34 and CD45 (Fig. 2F; Figure S2E). Trilineage differentiation analyses confirmed the multipotency of hPSC-NCC-MSC (Fig. 2G; Figure S2F). Adipocytes were visualized using Oil Red O staining after 2 weeks of differentiation, demonstrating comparable adipogenic capacity across groups. Similarly, osteoblasts derived from MSC were identified via Alizarin Red S staining, and chondrosphere formation was confirmed by Toluidine Blue staining. Moreover, qPCR revealed that hPSC-NCC-MSC exhibited elevated mRNA levels of osteogenic genes, including *ALP*, *OCN*, and *RUNX2*, compared to UC-MSC. However, adipogenic gene expression (*ADIPOQ*, *LPL*, *aP2*, and *PPAR-γ*) was comparable between hPSC-NCC-MSC and UC-MSC, suggesting that hPSC-NCC-MSC possessed enhanced osteogenic but not adipogenic differentiation potential relative to UC-MSC (Fig. 2H). Collectively, the two-stage differentiation protocol effectively generated hPSC-NCC-MSC with defined phenotypic characteristics and robust trilineage differentiation potential.

H1-NCC-MSC exhibited enhanced proliferative capacity and reduced cellular senescence compared to UC-MSC

H1-NCC-MSC derived from H1-hESC-NCC demonstrated superior long-term proliferative potential compared to both HEF-NCC-MSC (derived from HEF-iPSC-NCC) and UC-MSC (Fig. 2I), suggesting their potential as a promising candidate for the treatment of chemotherapy-induced POI. To further assess anti-senescence capacity, the proliferative abilities of H1-NCC-MSC and UC-MSC were compared at passages 4 and 15. CCK-8 assays revealed that H1-NCC-MSC maintained significantly higher proliferation rates at both passages than UC-MSC (Fig. 3A). Immunostaining for *Ki67* showed a marked reduction in *Ki67*-positive cells in

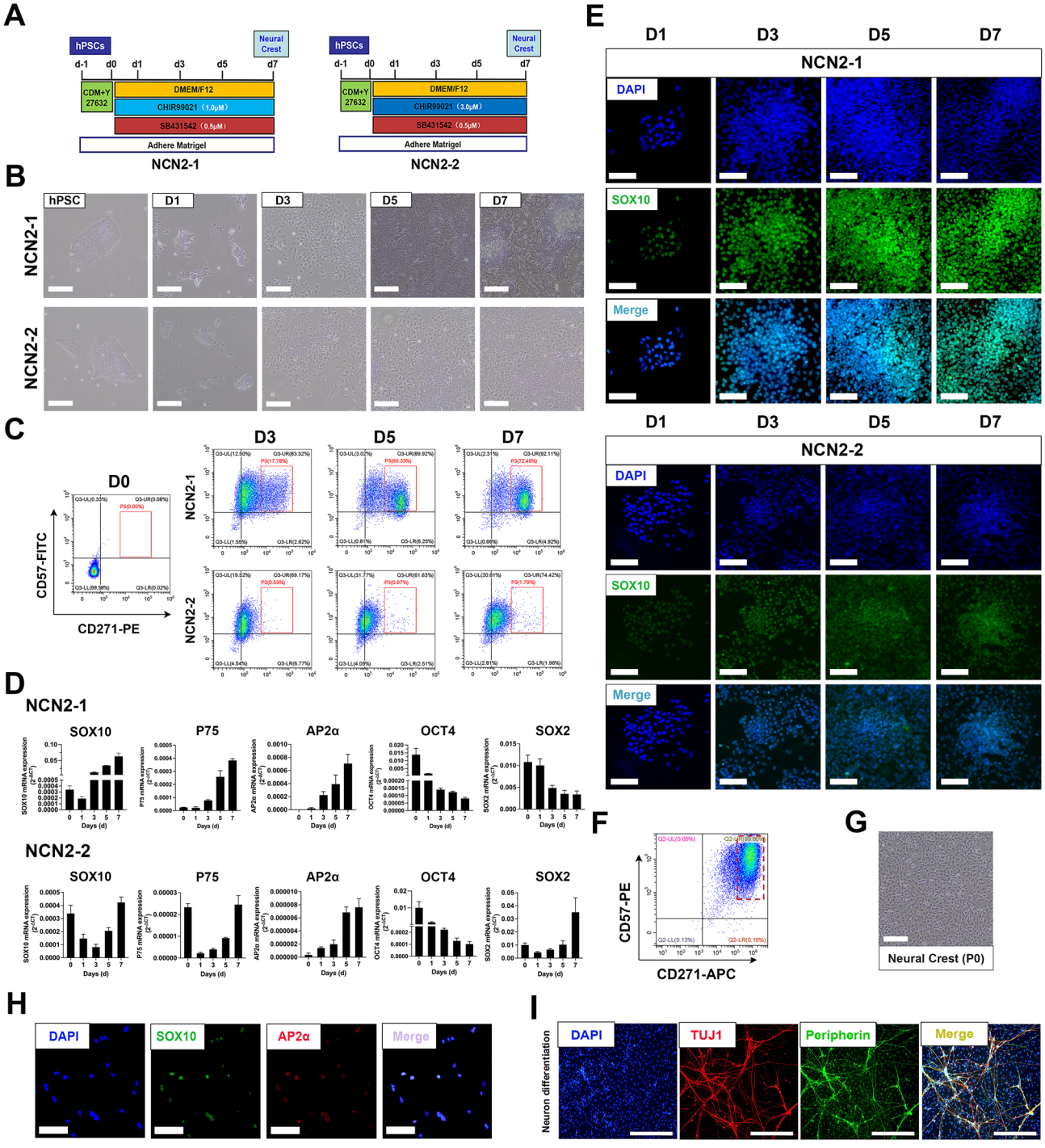

Fig. 1 Differentiation and characterization of human pluripotent stem cells-derived neural crest cells (hPSC-NCC). **A**. Illustration diagram of the two regimens for hPSC-NCC differentiation. **B**. Cell morphology in two induction regimens was shown on day 0, 1, 3, 5, 7. Scale bar: 500 μm. **C**. Flow cytometric analysis was performed to analyze CD271 (P75NTR) and CD57 (HNK1) in two induction regimens on day 0, 3, 5, 7. **D**. Specific NCC genes, P75, HNK1, SOX10 and AP2α mRNA levels in two induction regimens were analyzed using qPCR analysis on day 1, 3, 5, 7. **E**. Cells in two induction regimens immunostained for SOX10 on day 1, 3, 5, 7. Scale bar: 100 μm. **F-H**. $P75^{++}/HNK1^{+}$ enrichment hPSC-NCC were sorted by FACS, observed under microscope and immunostained for SOX10 and AP2α. Scale bar: 100 μm. **I**. Neurons derived from $P75^{++}/HNK1^{+}$ hPSC-NCC immunostained for TUJ1 and peripherin. Scale bar: 100 μm

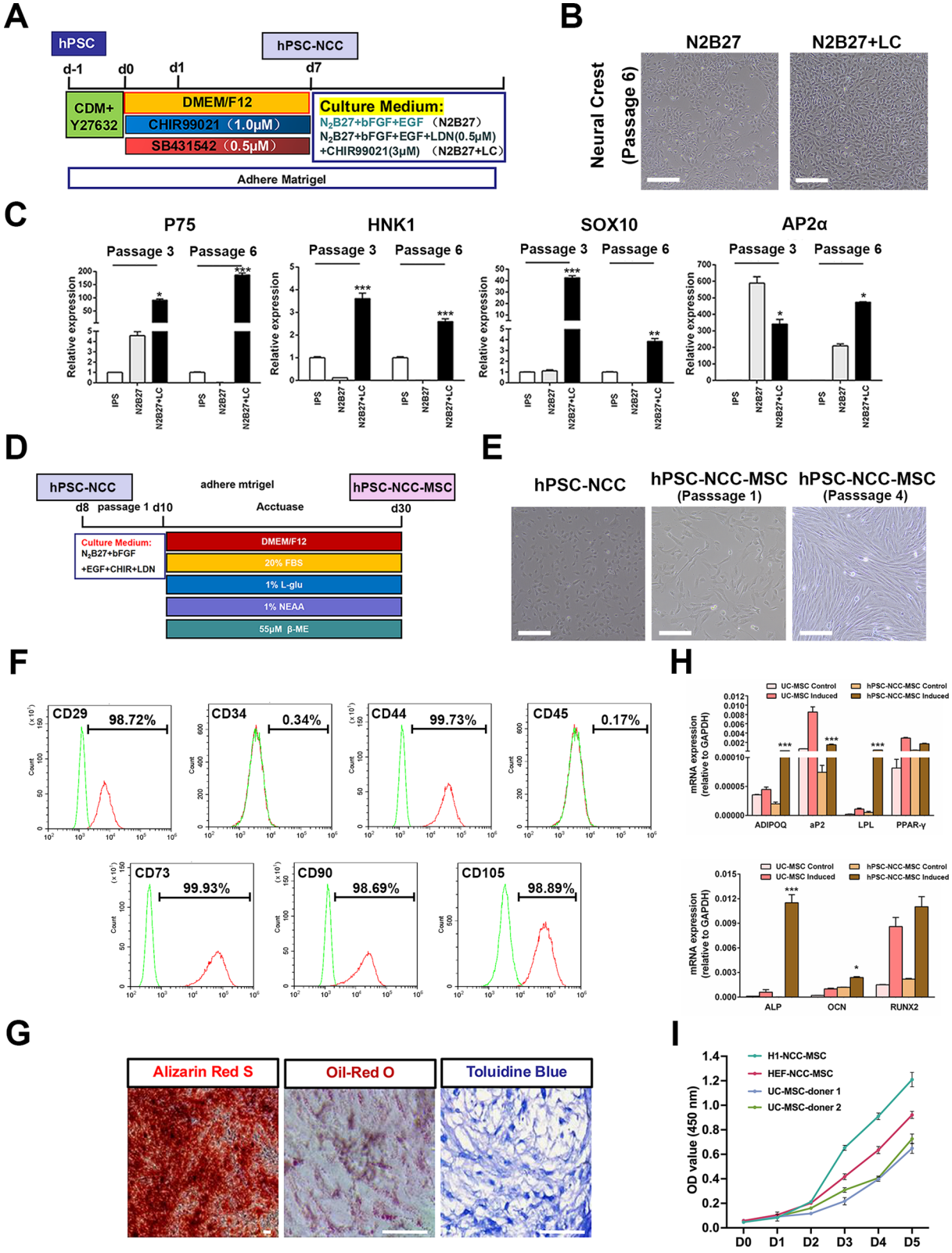

Fig. 2 (See legend on next page.)

(See figure on previous page.)

Fig. 2 Differentiation and identification of mesenchymal stem cells derived from hPSC-NCC (hPSC-NCC-MSC). **A**. Scheme illustration of two maintenance culture mediums of NCC. **B**. Cell morphology of hPSC-NCC at passage 6 in N2B27 and N2B27 + LC culture medium. Scale bar: 500 μm. **C**. NCC markers *P75*, *HNK1*, *SOX10* and *AP2α* mRNA levels of hPSC-NCC at passage 3 and 6 were analyzed by qPCR. $^{*}p < 0.05$, $^{**}p < 0.01$, $^{***}p < 0.001$ N2B27 vs. N2B27 + LC. **D**. Scheme illustration of hPSC-NCC-MSC differentiation. **E**. Cell morphology of H1-NCC and H1-NCC-MSC. Scale bar: 500 and 200 μm. **F**. Representative histograms for stem cell (CD29, CD44, CD73, CD90, CD105) and hematopoietic stem cell (CD34, CD45) surface markers of H1-NCC-MSC analyzed by flow cytometry. The green color indicates the isotype control group, while the red color represents the hPSC-NCC-MSC group. **G**. Trilineage differentiation of H1-NCC-MSC. Scale bar: 100 μm. **H**. Adipocyte and osteoblast related genes were analyzed by qPCR. $^{*}p < 0.05$, $^{**}p < 0.01$, $^{***}p < 0.001$ H1-NCC-MSC induced vs. UC-MSC induced. **I**. Cell proliferative rates were analyzed by CCK8 assay

UC-MSC at passage 15, whereas H1-NCC-MSC retained a consistent proportion of *Ki67*-positive cells across passages (Fig. 3B-E). Morphologically, H1-NCC-MSC maintained a uniform, elongated fusiform shape after 15 passages, while UC-MSC exhibited hypertrophy, irregular flattening, and a vacuolated appearance (Fig. 3F).

Increased SA-β-gal activity and elevated protein levels of senescence-associated markers (*γ-H2AX*, *P16*, and *P21*) were observed in UC-MSC at passage 15 compared to those at passage 4, whereas these markers remained stable in H1-NCC-MSC across passages (Fig. 3G-J). Overall, these results indicated that H1-NCC-MSC possessed a markedly enhanced proliferative capacity and anti-senescence potential, making them a superior resource for chemotherapy-induced POI treatment.

H1-NCC-MSC and UC-MSC transplantation improved ovarian function and structure in chemotherapy-induced POI rat model

The indicated interventions were administered to 7-week-old SD rats in various experimental groups (Fig. 4A). Following 14 days of continuous CTX injections, body weight significantly declined in the POI, UC-MSC, and H1-NCC-MSC groups compared to the control group, and subsequently improved over the following 22 days in the UC-MSC and H1-NCC-MSC groups (Fig. 4B). A similar trend was observed in estrous cycle recovery, as irregular cycles in the MSC-treated groups normalized post-transplantation, while the POI group remained abnormal (Fig. 4C; Figure S3). Ovarian volume and weight, which were markedly reduced in the POI group compared to controls, were effectively restored in the MSC-treated groups (Fig. 4D–E). H&E staining revealed that the control group ovaries contained abundant follicles at various developmental stages. In contrast, the POI group exhibited a sharp decline in follicle numbers, particularly primordial follicles. MSC transplantation partially restored the follicle count (Fig. 4F–G). Consistently, mRNA expression of folliculogenesis-related genes (*Amh*, *Bmp15*, *Gdf9*, and *Foxl2*) was significantly upregulated following MSC treatment, aligning with the observed follicle recovery (Figure S4). Hormone analysis showed that estradiol (E_2) and anti-Müllerian hormone (AMH) levels, which were reduced by CTX, were increased following MSC therapy, while follicle-stimulating hormone (FSH) levels exhibited the opposite trend (Fig. 4H). Fertility assessment revealed that the litter size in the MSC-treated groups was significantly larger than in the POI group (Fig. 4I–J). Finally, safety evaluations indicated no in vivo toxicity associated with H1-NCC-MSC transplantation (Figure S5). The above results suggested that H1-NCC-MSC and UC-MSC transplantation can partially mitigate chemotherapy-induced ovarian damage. However, no significant differences were observed in therapeutic efficacy between the two MSC types.

H1-NCC-MSC and UC-MSC demonstrated viability improvement and apoptosis Inhibition effects on GC in vivo

We further explored the underlying mechanisms of MSC on damaged GC. First, far-red plasma membrane fluorescent tracer DID was used to confirm the ovarian distribution of transplanted MSC. UC-MSC and H1-NCC-MSC exhibited spatiotemporal heterogeneity in ovarian biodistribution. Results showed that UC-MSC predominance in the medullary region, whereas H1-NCC-MSC were mainly localized in peri-follicular niches adjacent to theca cells. Notably, some H1-NCC-MSC were also scattered in the ovarian medulla. (Fig. 5A). TUNEL staining revealed a significant presence of TUNEL-positive GC (green) in the ovaries of the POI group. Three weeks after H1-NCC-MSC or UC-MSC transplantation, TUNEL-positive GC were dramatically diminished (Fig. 5B-C). Meantime, IHC staining demonstrated decreased *PCNA* expression in damaged GC of the POI group, which was restored following H1-NCC-MSC or UC-MSC treatment. However, no statistically significant difference was observed between H1-NCC-MSC and UC-MSC groups in these outcomes (Fig. 5D-E).

Conditioned medium (CM) of H1-NCC-MSC and UC-MSC promoted GC viability in vitro

Given that transplanted MSC localized near but did not migrate into follicles, it was inferred that GC repair was mediated through paracrine mechanisms rather than direct differentiation into follicular cells. To validate this hypothesis, the conditioned medium (CM) from both MSC types was used to assess their effects on GC in vitro. KGN cells exposed to 4-HC displayed abnormal and irregular morphology, which was partially restored to a fibroblast-like appearance after treatment with CM from H1-NCC-MSC or UC-MSC (Fig. 5F). Annexin V/

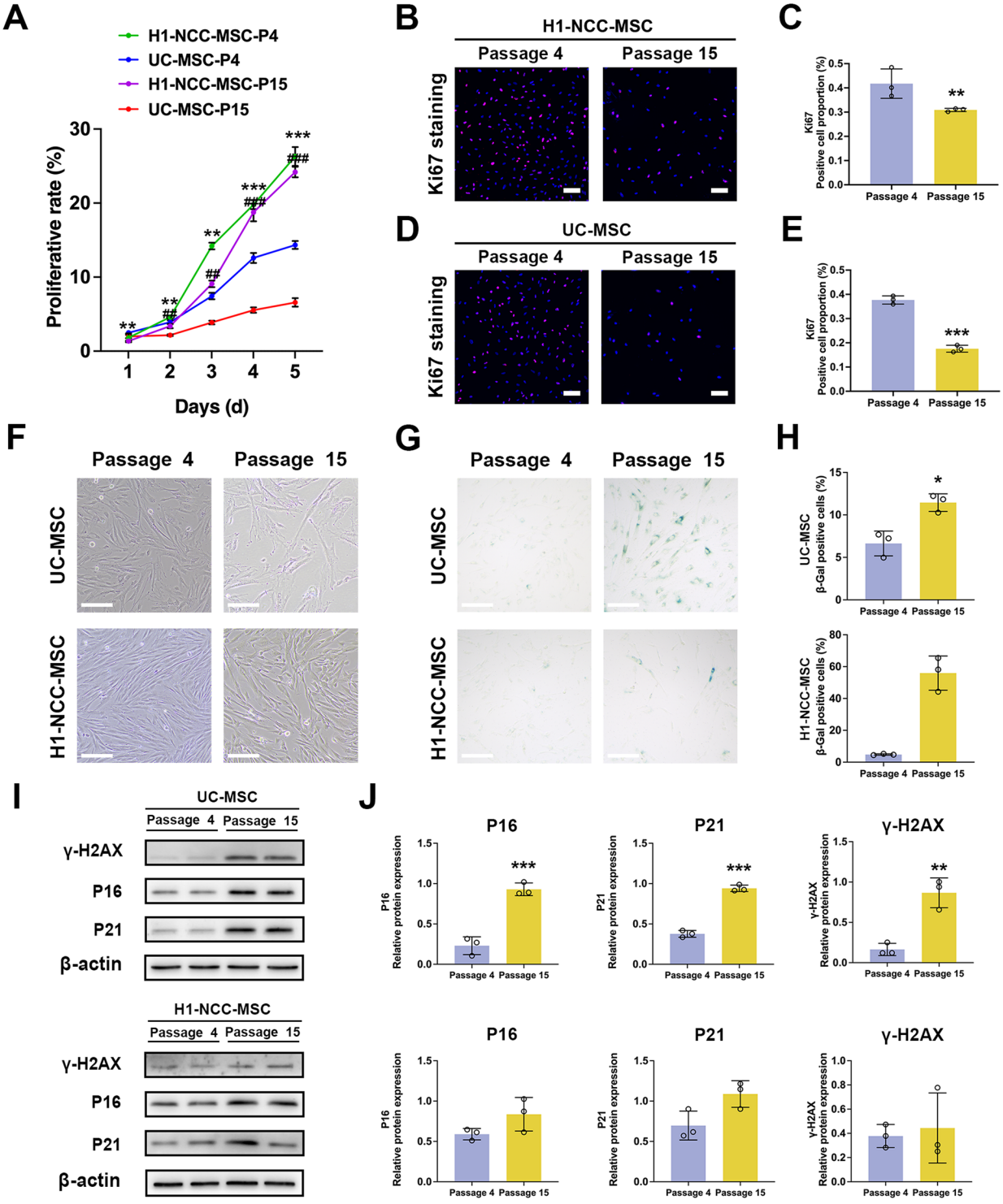

Fig. 3 Comparison of viability and anti-senescence capability between H1-NCC-MSC and UC-MSC at different passages. **A**. Cell proliferative rates were analyzed by CCK8 assay. $^{**}p < 0.01$, $^{***}p < 0.001$ H1-NCC-MSC Passage 4 (P4) vs. UC-MSC Passage 4 (P4); $^{\#\#}p < 0.01$, $^{\#\#\#}p < 0.001$ H1-NCC-MSC Passage 15 (P15) vs. UC-MSC Passage 15 (P15). **B-E**. *Ki67* immunostaining and quantitative analysis of *Ki67* positive cell proportion ($n = 3$). Scale bar: 100 μm. **F**. Cell morphology. Scale bar: 200 μm. **G-H**. Representative images of aging-related β-galactosidase staining and quantitative analysis of positive cells ($n = 3$). Scale bar: 200 μm. **I-J**. *γ-H2AX*, *P21* and *P16* protein levels were quantified by Western blotting ($n = 3$). $^{*}p < 0.05$, $^{**}p < 0.01$, $^{***}p < 0.001$. Full-length blots are presented in Additional file 2: Figure S6

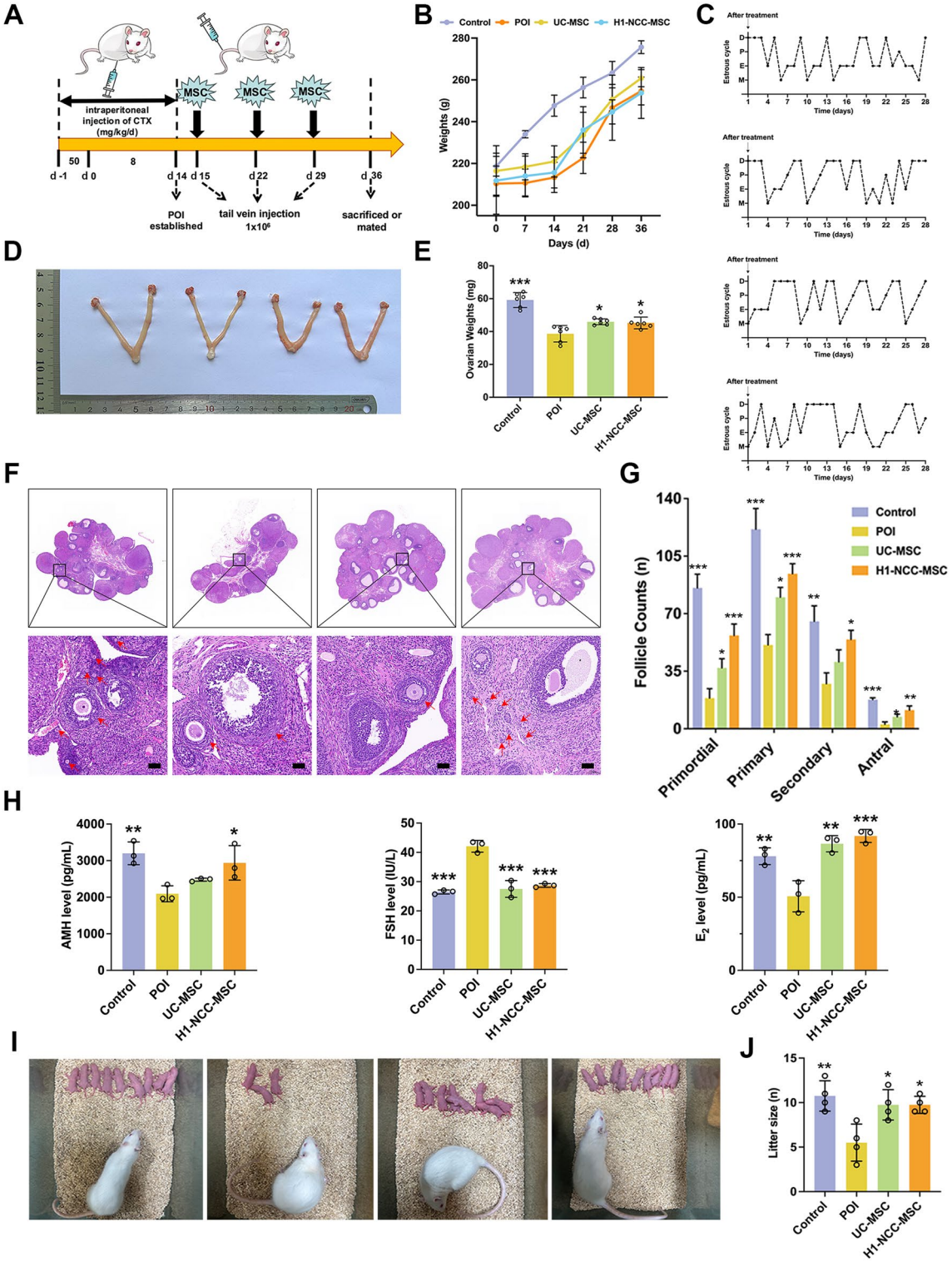

Fig. 4 H1-NCC-MSC and UC-MSC transplantation improved the ovarian function and structure of chemotherapy induced POI rat model. **A**. Illustration diagram of in vivo experiment. **B**. Body weight (g). **C**. Estrous cycles were analyzed using vaginal cytology. **D**. Gross image of ovaries. **E**. Bilateral ovarian weight (mg) ($n = 3$). **F-G**. Ovarian structure and follicle counts were evaluated by H&E staining ($n = 3$). Arrow points to follicles at different stages. Scale bar: 50 μm. **H**. AMH, FSH and E_2 levels ($n = 3$). **I-J.** Fertility assessment was evaluated by litter size ($n = 4$). $^{*}p < 0.05$, $^{**}p < 0.01$, $^{***}p < 0.001$ vs. POI group

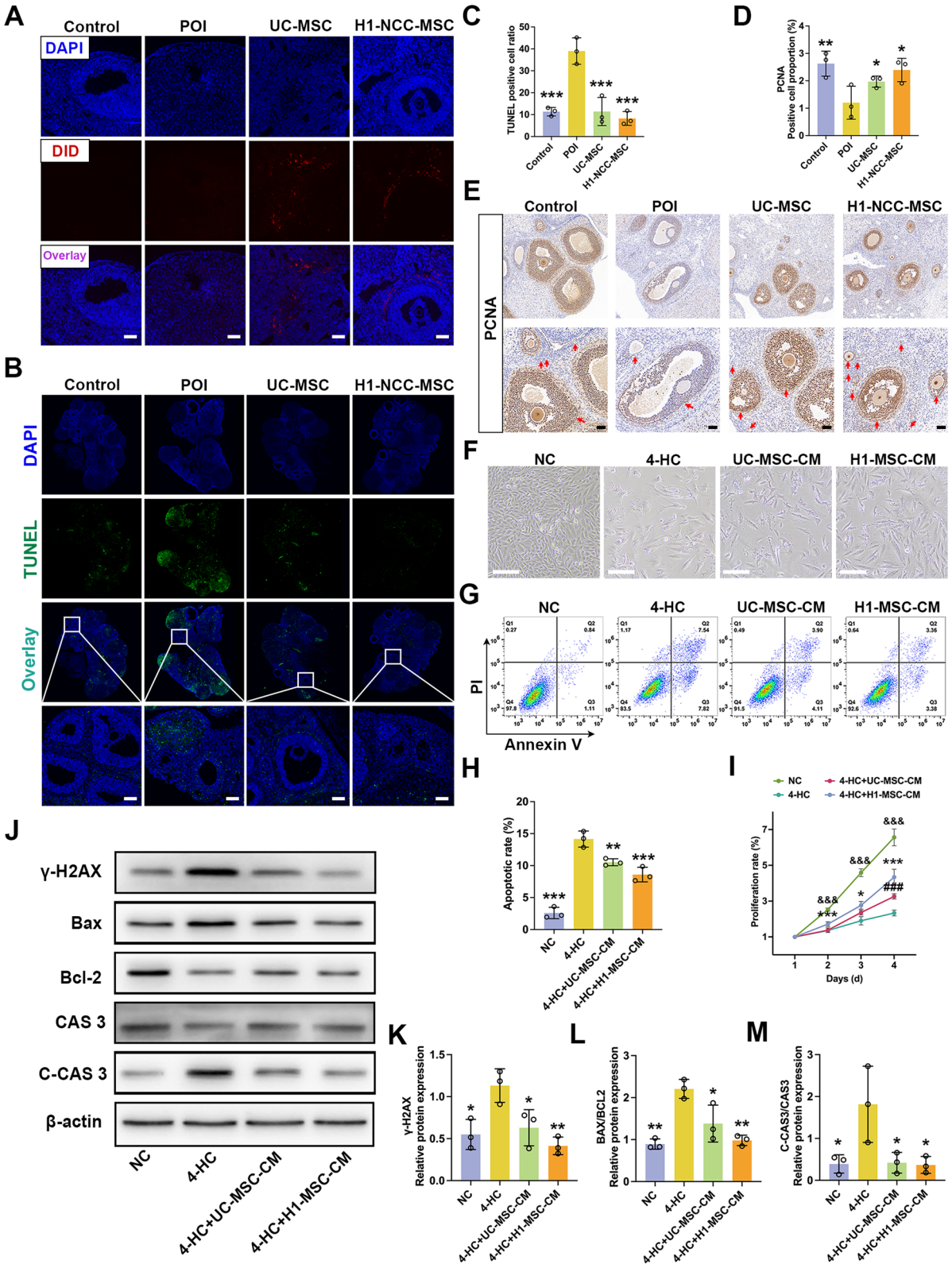

Fig. 5 (See legend on next page.)

(See figure on previous page.)

Fig. 5 H1-NCC-MSC and UC-MSC asserted pro-viability and anti-apoptosis effect on GC in vivo and *in vitro*.**A**. MSC tracking in ovaries by DID-fluorescence probe. Scale bar: 100 μm. **B-C**. Apoptotic ovarian GC were evaluated by TUNEL assay and quantitative analysis of TUNEL positive cell ratio was conducted ($n=3$). Scale bar: 100 μm. **D-E.** Proliferation indicator *PCNA* was immunostained and quantitative analysis was conducted for ovarian *PCNA* positive cells ($n=3$). Scale bar: 50 μm. **F**. KGN cell morphology. Scale bar: 200 μm. **G-H**. Apoptotic rates of KGN detected using flow cytometry and quantitative analysis was conducted ($n=3$). **I**. Proliferation rates were analyzed by CCK8. $^{*}p<0.05$, $^{***}p<0.001$ 4-HC + H1-MSC-CM vs. 4-HC group; $^{\&\&\&}p<0.001$ NC vs. 4-HC group; $^{\#\#\#}p<0.001$ 4-HC + UC-MSC-CM vs. 4-HC group. **J-M**. Protein levels of apoptosis-related genes *γ-H2AX*, *BAX*, *BCL-2*, *Caspase 3 (CAS3)* and *Cleaved caspase 3 (C-CAS3)* were quantified by Western blotting ($n=3$). $^{*}p<0.05$, $^{**}p<0.01$, $^{***}p<0.001$ vs. POI or 4-HC group. Full-length blots are presented in Additional file 2: Figure S7-S8.

PI assays revealed that elevated apoptotic rates of KGN cells induced by 4-HC were significantly lower after co-cultured with either UC-MSC-CM or H1-MSC-CM (Fig. 5G-H). Similarly, CCK8 assays confirmed that CM from both MSC types enhanced KGN cell viability (Fig. 5I). Consistently, increased protein levels of *γ-H2AX*, *BAX*/*BCL-2* and *Cleaved Caspase-3/Caspase-3 (C-CAS3/CAS3)* were found in 4-HC group compared to those in the MSC-CM treated groups (Fig. 5J-M). No significant difference in efficacy was detected between H1-MSC-CM and UC-MSC-CM treatments.

H1-MSC-CM and UC-MSC-CM ameliorated oxidative stress and mitochondrial damage of GC in vitro

As oxidative stress is a critical factor in cyclophosphamide (CTX)-induced ovarian injury, which disrupts antioxidant defense mechanisms and generates excessive malondialdehyde (MDA) [20], it was hypothesized that H1-NCC-MSC exerts antioxidant effects in KGN cells. The DCFH-DA assay demonstrated elevated ROS levels across all 4-HC-treated groups, with UC-MSC-CM and H1-MSC-CM treatments significantly mitigating ROS accumulation (Fig. 6A). JC-1 staining indicated a rapid depolarization of mitochondrial membrane potential (MMP) in the 4-HC group, which was reversed by H1-MSC-CM and UC-MSC-CM treatment (Fig. 6B). Moreover, mitochondrial ROS levels were quantified using MitoSOX Red staining. Consistent with the DCFH-DA results, flow cytometry and fluorescence microscopy revealed an accumulation of mitochondrial ROS in the 4-HC group, which was markedly reduced by H1-MSC-CM and UC-MSC-CM treatments (Fig. 6C-E). Levels of oxidative MDA, as well as antioxidant markers glutathione (GSH) and superoxide dismutase (SOD), were also assessed. MDA levels were significantly increased in cells of the 4-HC group compared to the NC group, whereas treatment with H1-MSC-CM and UC-MSC-CM reduced MDA levels in a dose-dependent manner. Conversely, GSH and SOD levels were significantly elevated following these treatments (Fig. 6F-H). These findings highlight the ability of H1-MSC-CM and UC-MSC-CM to reduce oxidative stress and mitochondrial dysfunction.

Discussion

Premature ovarian insufficiency (POI), a common condition leading to ovarian dysfunction, poses a serious threat to women's reproductive health. Despite the absence of effective treatments, regenerative medicine has made a remarkable progress in addressing POI. Accumulative studies have shown that MSC has excellent therapeutic potential for POI treatment [21]. However, challenges persist in the clinical application of MSC therapies. One major issue is the heterogeneity in MSC sources, which significantly impacts therapeutic efficacy. Additional factors such as donor age and intrinsic donor-to-donor MSC variability further complicate clinical outcomes. Consequently, alternative cell sources capable of producing standardized, renewable, and functional MSC populations are urgently needed.

Recent studies have proven that MSC derived from hPSC represent a homogeneous and promising source for ovarian reserve restoration, with the intermediate stages of hPSC-MSC predominantly restricted to the mesoderm [22–24]. While neural crest cells (NCC) have been shown to developmentally differentiate into MSC subpopulations [25], limited research has explored the derivation of MSC from hPSC via NCC. As well known, NCC are a transient cell population with stem cell-like properties that emerge from the dorsal neural plate border during vertebrate embryogenesis [26]. Notably, NCC have been detected in the ovaries of mouse embryos at E16.5, where they incrementally differentiate into neurons, invade the dorsal surface during postnatal development, and contribute to the regulation of ovarian neuroendocrine functions [11]. Besides, ovarian Leydig cells may originate from the neuroectoderm of NCC, further underscoring their potential role in ovarian function [27]. Consequently, hPSC-derived NCC may serve as an ideal source for ovarian repair. Traditionally, differentiation of hPSC into NCC via embryoid body (EB) formation has been a time-consuming and inefficient process [28]. A more efficient approach has been developed using CHIR99012 and SB431542 to induce NCC from human embryonic stem cells (hESC) or induced pluripotent stem cells (hiPSC) [29]. CHIR99021, a glycogen synthase kinase 3 beta (GSK-3β) inhibitor, activates the canonical Wnt/β-catenin pathway [30], which plays a crucial role in neural tissue patterning [31]. Concurrently, the TGF-β inhibitor SB431542 enhances the efficiency of neural induction by

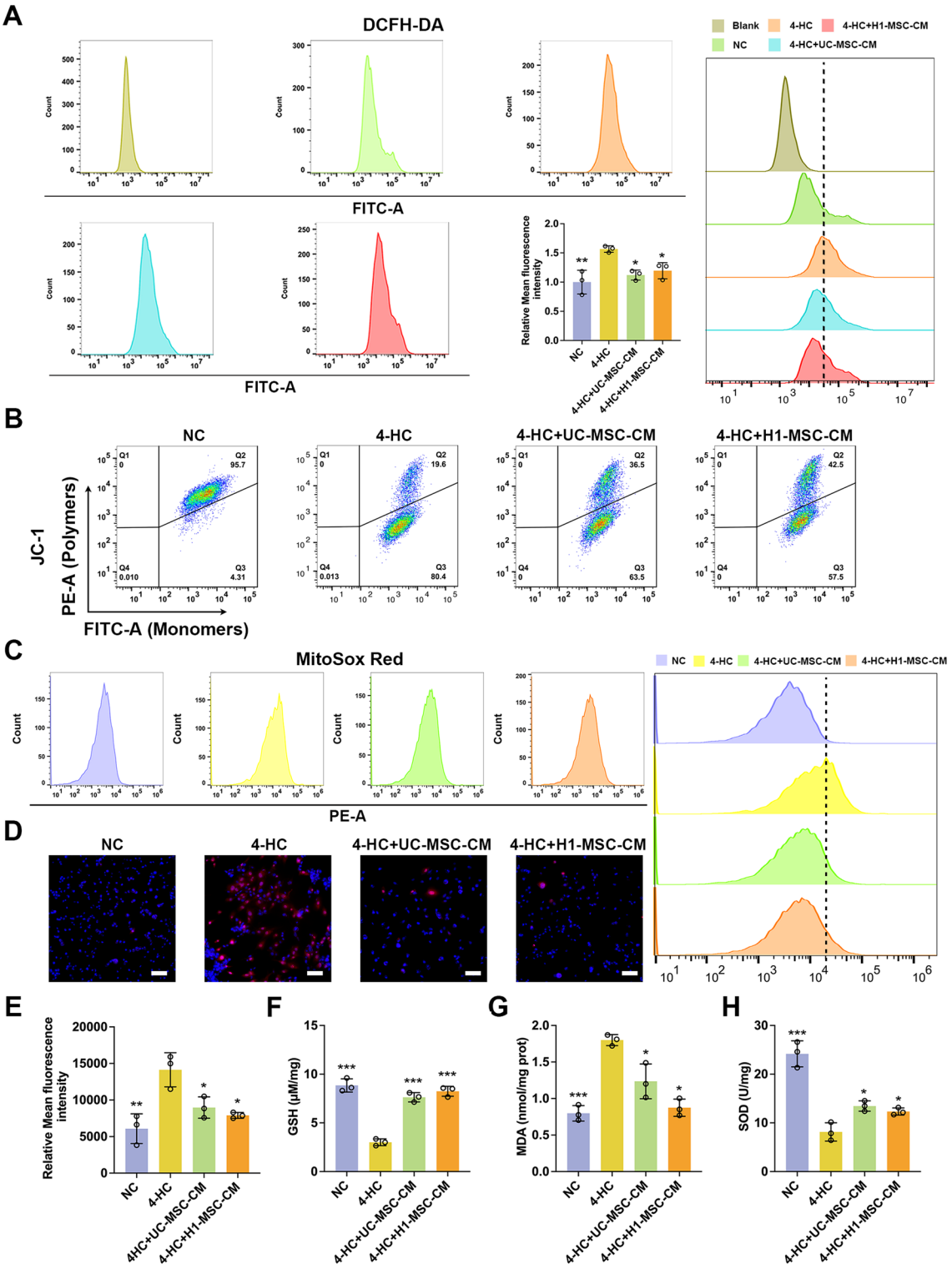

Fig. 6 Conditioned medium (CM) of H1-NCC-MSC and UC-MSC ameliorated oxidative stress and mitochondrial damage of GC in vitro. **A**. ROS concentrations in KGN cells were detected by flow cytometry using DCFH-DA and quantitative analysis was conducted for mean fluorescence intensity (MFI) ($n = 3$). **B**. Mitochondrial membrane potential (MMP) was detected by flow cytometry using JC-1 assay ($n = 3$). **C-D**. Mitochondrial ROS levels were detected by flow cytometry and observed under fluorescence microscope using MitoSOX Red staining. Scale bar: 100 μm. **E**. Quantitative analysis was conducted for mitochondrial ROS levels. **F-H.** MDA, GSH and SOD levels in KGN cells lysates ($n = 3$). *$P < 0.05$, **$P < 0.01$, ***$P < 0.001$ compared with the 4-HC group

blocking phosphorylation of ALK4/5/7 receptors [32]. In line with a previous study [33], a modified dual-inhibitor method was employed for the induction of neural crest cells (NCC) from human pluripotent stem cells (hPSC), including H1-hESC, H9-hESC, and HEF-iPSC. Using 1 μM CHIR99012 and 0.5 μM SB431542, the hPSC successfully differentiated into NCC with functional phenotypes within the first seven days. This differentiation was characterized by the upregulation of typical NCC markers (*P75*, *HNK1*, *SOX10*, and *AP2α*) and the downregulation of pluripotency markers (*SOX2* and *OCT4*). To the best of our knowledge, the SB431542 concentration used in this study was lower than that reported in other publications [29, 34]. Simultaneously, a preferred NCC maintenance medium comprised LDN-193189 was initially introduced in our study, demonstrating efficacy in preserving NCC characteristics. LDN-193189, a specific inhibitor of type I BMP receptors, enhances NCC formation by suppressing BMP/Smad signaling [35], indicating its essential role in maintaining NCC phenotypes. Previous study has proven that hiPSC represent a more potential source of various terminally differentiated cells when compared to hESC, due to their self-derived transplantation capability [6]. On the contrary, our study confirmed that H1-hESC (72.45%) certainly displayed the highest induction efficiency compared to H9-hESC (40.99%) and HEF-iPSC (69.15%). Correspondingly, H1-NCC-MSC manifested higher proliferative rates than HEF-NCC-MSC. Interestingly, other studies have approved that serum-free medium can effectively induce hPSC-NCC-MSC [29, 36]. However, in this study, the use of serum-free media failed to produce relevant NCC (data not shown), which may be attributed to the lower concentration of SB431542 used. Further investigations are required to optimize SB431542 concentration for efficient NCC induction under serum-free medium.

Notably, H1-NCC-MSC demonstrated a more pronounced naïve phenotype relative to UC-MSC, a phenomenon that may be explained through comprehensive aspects. The reprogramming process from somatic cells to hPSC-MSC resets the epigenetic landscape of the cells, returning them to a pluripotent, embryonic-like state, theoretically preserving some pluripotency traits of the original iPSC [37]. However, UC-MSC are directly isolated from neonatal umbilical cord tissue and are considered adult stem cells. Their epigenetic modifications and differentiation potential are influenced by heterogeneity such as the donor's age and the tissue microenvironment. On the other hand, during the reprogramming process, iPSC erase the epigenetic memory of the somatic cells and adopt an open chromatin state similar to that of embryonic stem cells [38]. This epigenetic reset could potentially endow hPSC-MSC with greater plasticity during differentiation.

Consistent with the results of our study, several studies have shown that hPSC-MSC exhibit superior proliferation rates and anti-senescence capability compared to adult tissue-derived MSC. Kimbrel et al. found that hPSC-MSC exhibit over 30,000 times proliferative rates and significant smaller sizes than those of bone marrow-derived MSC (BMSC) [39, 40]. Additionally, Tian et al. suggested that hPSC-derived MSC showed excellent proliferation speed and reduced aging over 10 passages [41]. In contrast, adult MSC began to enlarge at passage 5, and represented a 4.8-fold larger size at passage 9 compared with passage 1 [42]. At late passages during culture, the expression of Senescence-Associated Secretory Phenotype (SASP) factors is also increased, which drives responses that reinforce senescence [43, 44]. Collectively, hPSC-MSC exhibit a more primitive differentiation state compared to adult tissue-derived MSC, as evidenced by their retained naïve pluripotency-associated transcriptional signatures, primed epigenetic configurations, robust proliferative rates and superior anti-senescence capability.

Thereafter, we utilized H1-NCC-MSC and UC-MSC, both of which were administered via multidose of intravenous injection, and drew comparisons of their therapeutic efficacy in CTX-induced POI. Our data showed that both H1-NCC-MSC and UC-MSC were capable of restoring ovarian function by upregulating the expression of proliferating cell nuclear antigen (*PCNA*) and inhibiting apoptosis in ovarian granulosa cells (GC), leading to successful pregnancies in the chemotherapy-induced POI rat model. However, neither H1-NCC-MSC nor UC-MSC restored the ovaries to their normal physiological state, and no statistically significant differences in therapeutic efficacy were observed between the two MSC types. It is hypothesized that the limited efficacy may be attributed to the deleterious microenvironment in CTX-damaged ovaries, which is unfavorable for the long-term survival and functional integration of transplanted cells [45]. Though the underlying mechanisms of chemotherapy-induced POI are still ambiguous, CTX is believed to induce excessive oxidative stress, increasing reactive oxygen species (ROS) production while suppressing antioxidant biosynthesis, such as glutathione (GSH) and superoxide dismutase (SOD) [46]. ROS acts as a signal molecule and plays a crucial role in regulating various reproductive processes but can cause overproduction of oxidative products like malondialdehyde (MDA). In contrast, SOD converts superoxide radicals into molecular oxygen and hydrogen peroxide [47], and GSH serves as a fundamental molecule for regulating cellular redox homeostasis [48]. Mitochondria in ovarian GC are essential for supporting oocyte development [49]. Excessive ROS generated by oxidative stress leads to mitochondrial dysfunction, driving inflammation [50] and pyroptosis

[51] in ovarian GC. Therefore, mitigating oxidative stress is critical to improving the therapeutic efficacy of MSC-based treatments. In agreement with previous studies [52], H1-NCC-MSC and UC-MSC were primarily localized around, rather than within, ovarian follicles in this study, suggesting that their therapeutic effects may be mediated through paracrine mechanisms. Recent studies have shown that exosomes secreted by human amniotic MSC (hAMSC) or human pluripotent stem cell-derived MSC (hPSC-MSC) reduce ROS levels in GC and oocytes in CTX-induced POI models [53, 54]. Aligning with these findings, we chose conditioned medium (CM) of the two MSC as a substitute to explore whether it posts an essential role in ameliorating oxidative stress. H1-MSC-CM not only increased GSH and SOD levels but also reduced the expression of oxidative products such as ROS and MDA. Evaluation of mitochondrial function revealed that mitochondrial membrane potential (MMP), a critical marker of mitochondrial integrity, was significantly decreased in the CTX-treated (4-HC) group but was restored after treatment with CM from both H1-NCC-MSC and UC-MSC. The mitochondrial ROS levels followed a trend similar to that of MMP. Encouragingly, although no statistically significant differences in oxidative stress reduction were observed between the CM from H1-NCC-MSC and UC-MSC, H1-NCC-MSC demonstrated superior efficacy in inhibiting apoptosis and ameliorating oxidative stress. Further studies with larger sample sizes are warranted to elucidate the precise mechanisms underlying the therapeutic effects of H1-NCC-MSC, which will aid in optimizing its clinical application.

Despite the promising findings, this study still has several limitations. First, the use of FBS-containing culture medium hinders the clinical application of H1-NCC-MSC, necessitating the development of an induction process utilizing xeno-free medium. Second, comparisons among hPSC-MSC derived from different intermediate differentiation stages could not be performed, limiting insights into their relative therapeutic potential. Third, the underlying mechanisms of H1-NCC-MSC treatment in the CTX-induced POI model remain insufficiently elucidated.

Conclusion

Our study provides previously unpublished evidence that hPSC-NCC-MSC improve chemotherapy-induced POI both in vivo and in vitro by promoting GC viability, suppressing apoptosis, and alleviating oxidative stress. Although hPSC-NCC-MSC do not exhibit superior therapeutic effects compared to UC-MSC, their robust viability and renewable source position them as a promising candidate for MSC-based therapies. These findings present compelling experimental evidence supporting the clinical application of hPSC-NCC-MSC for the treatment of POI.

Abbreviations

POI	Premature ovarian insufficiency
FSH	Follicle-stimulating hormone
MSC	Mesenchymal stem cells
UC-MSC	Umbilical cord mesenchymal stem cells
GC	Granulosa cells
hPSC	Human pluripotent stem cells
hiPSC	Human induced pluripotent stem cells
hESC	Human embryonic stem cells
NCC	Neural crest cells
SA-β-Gal	Senescence-Associated β-galactosidase
CTX	Cyclophosphamide
4-HC	4-Hydroperoxy cyclophosphamide
H&E	Hematoxylin and eosin
qPCR	Quantitative real-time polymerase chain reaction
FCM	Flow cytometry
FACS	Fluorescence-activated cell sorting
E_2	Estradiol
AMH	Anti-Müllerian hormone
SOD	Superoxide dismutase
MDA	Malondialdehyde
GSH	Glutathione
WB	Western blotting

Supplementary Information

The online version contains supplementary material available at https://doi.org/10.1186/s13287-025-04346-x.

Supplementary Material 1

Supplementary Material 2

Acknowledgements

We are grateful for the kind and generous provision of cell lines by Professor Xiafei Fu from Zhujiang Hospital affiliated with Southern Medical University. Here, we declare that all authors have not use AI-generated work in this manuscript.

Author contributions

Huiyan Wang participated in the overall experimental design. Xinran Li conducted both in vivo and in vitro experiments and was the major contributor to writing the manuscript. JR Liao analyzed and interpreted the experimental data. Youhong Zheng was responsible for all illustrations. Yifeng Wang and Xuefeng Wang were responsible for revising the manuscript draft. All authors read and approved the final manuscript.

Funding

This work was supported by grants from the National Natural Science Foundation of China (CN) (82001501) and the Undergraduate Innovative Training Project of Southern Medical University (202412121335).

Data availability

All data generated or analyzed during this study are included in the published article and its supplementary information files.

Declarations

Ethics approval and consent to participate

hPSC cell lines (hESC and HEF-iPSC) were all donated by Professor Xiafei Fu. The hESC (WA01/WA09) were commercially purchased from WiCell Research Institute, USA. Besides, the HEF-iPSC were derived from WI-38 human embryonic fibroblast (ATCC, USA). All cell lines were obtained with documented ethical compliance, including institutional ethics approval and donor informed consent. UC-MSC used in this study were obtained from healthy donors with prior informed consent and approved by the Medical Ethics Committee of Zhujiang Hospital affiliated with Southern Medical

University (Title: Assessment of the efficacy and mechanisms of MSC from different developmental origins in POI treatment; Approval Number: 2023-KY-125-01; Date of approval: 21/07/2023). Animal studies were conducted in compliance with the recommendations in the Guide for the Care and Use of Laboratory Animals of the National Institutes of Health. All procedures were approved by the Committee on the Ethics of Animal Experiments of Zhujiang Hospital affiliated with Southern Medical University (Title: Assessment of the efficacy and mechanisms of MSC from different developmental origins in POI treatment; Approval Number: LAEC-2022-170; Date of approval: 22/11/2022).

Consent for publication
All authors have approved the manuscript and agreed with its submission.

Competing interests
The authors have no conflicts of interest.

Author details
[1]Obstetrics and Gynecology Center, Zhujiang Hospital, Southern Medical University, Guangzhou, Guangdong, China
[2]Department of Obstetrics and Gynecology, The Third Affiliated Hospital, Southern Medical University, Guangzhou, Guangdong, China
[3]Department of Obstetrics and Gynecology, The First People's Hospital of Foshan, Foshan, Guangdong, China

Received: 4 December 2024 / Accepted: 15 April 2025
Published online: 13 May 2025

References

1. Webber L, Davies M, Anderson R, Bartlett J, Braat D, Cartwright B, et al. ESHRE guideline: management of women with premature ovarian insufficiency. Hum Reprod. 2016;31:926–37.
2. Fraison E, Crawford G, Casper G, Harris V, Ledger W. Pregnancy following diagnosis of premature ovarian insufficiency: a systematic review. Reprod Biomed Online. 2019;39:467–76.
3. Shareghi-Oskoue O, Aghebati-Maleki L, Yousefi M. Transplantation of human umbilical cord mesenchymal stem cells to treat premature ovarian failure. Stem Cell Res Ther. 2021;12:454.
4. Bernardo ME, Fibbe WE. Mesenchymal stromal cells: sensors and switchers of inflammation. Cell Stem Cell. 2013;13:392–402.
5. Jiang T, Xu G, Wang Q, Yang L, Zheng L, Zhao J, et al. In vitro expansion impaired the stemness of early passage mesenchymal stem cells for treatment of cartilage defects. Cell Death Dis. 2017;8:e2851.
6. Takahashi K, Tanabe K, Ohnuki M, Narita M, Ichisaka T, Tomoda K, et al. Induction of pluripotent stem cells from adult human fibroblasts by defined factors. Cell. 2007;131:861–72.
7. Prakash N, Kim J, Jeon J, Kim S, Arai Y, Bello AB, et al. Progress and emerging techniques for biomaterial-based derivation of mesenchymal stem cells (MSCs) from pluripotent stem cells (PSCs). Biomater Res. 2023;27:31.
8. Yamanaka S. Pluripotent stem cell-Based cell Therapy-Promise and challenges. Cell Stem Cell. 2020;27:523–31.
9. Chijimatsu R, Ikeya M, Yasui Y, Ikeda Y, Ebina K, Moriguchi Y et al. Characterization of Mesenchymal Stem Cell-Like Cells Derived From Human iPSCs via Neural Crest Development and Their Application for Osteochondral Repair. Stem Cells Int. 2017;2017:1960965.
10. Mizoguchi T, Pinho S, Ahmed J, Kunisaki Y, Hanoun M, Mendelson A, et al. Osterix marks distinct waves of primitive and definitive stromal progenitors during bone marrow development. Dev Cell. 2014;29:340–9.
11. McKey J, Bunce C, Batchvarov IS, Ornitz DM, Capel B. Neural crest-derived neurons invade the ovary but not the testis during mouse gonad development. Proc Natl Acad Sci U S A. 2019;116:5570–5.
12. Mork L, Maatouk DM, McMahon JA, Guo JJ, Zhang P, McMahon AP, et al. Temporal differences in granulosa cell specification in the ovary reflect distinct follicle fates in mice. Biol Reprod. 2012;86:37.
13. Cordeiro MH, Kim SY, Ebbert K, Duncan FE, Ramalho-Santos J, Woodruff TK. Geography of follicle formation in the embryonic mouse ovary impacts activation pattern during the first wave of folliculogenesis. Biol Reprod. 2015;93:88.
14. Malamed S, Gibney JA, Ojeda SR. Ovarian innervation develops before initiation of folliculogenesis in the rat. Cell Tissue Res. 1992;270:87–93.
15. Dees WL, Hiney JK, McArthur NH, Johnson GA, Dissen GA, Ojeda SR. Origin and ontogeny of mammalian ovarian neurons. Endocrinology. 2006;147:3789–96.
16. Robker RL, Hennebold JD, Russell DL. Coordination of ovulation and oocyte maturation: A good egg at the right time. Endocrinology. 2018;159:3209–18.
17. Lv X, Guan C, Li Y, Su X, Zhang L, Wang X, et al. Effects of single and multiple transplantations of human umbilical cord mesenchymal stem cells on the recovery of ovarian function in the treatment of premature ovarian failure in mice. J Ovarian Res. 2021;14:119.
18. Wang Z, Wei Q, Wang H, Han L, Dai H, Qian X et al. Mesenchymal Stem Cell Therapy Using Human Umbilical Cord in a Rat Model of Autoimmune-Induced Premature Ovarian Failure. Stem Cells Int. 2020;2020:3249495.
19. Chen Y, Ai L, Zhang Y, Li X, Xu S, Yang W, et al. The EZH2-H3K27me3 axis modulates aberrant transcription and apoptosis in cyclophosphamide-induced ovarian granulosa cell injury. Cell Death Discov. 2023;9:413.
20. Helsby NA, Yong M, van Kan M, de Zoysa JR, Burns KE. The importance of both CYP2C19 and CYP2B6 germline variations in cyclophosphamide pharmacokinetics and clinical outcomes. Br J Clin Pharmacol. 2019;85:1925–34.
21. Sadeghi S, Mosaffa N, Huang B, Ramezani Tehrani F. Protective role of stem cells in POI: current status and mechanism of action, a review Article. Heliyon. 2024;10:e23271.
22. Cao RC, Lv Y, Lu G, Liu HB, Wang W, Tan C, et al. Extracellular vesicles from iPSC-MSCs alleviate chemotherapy-induced mouse ovarian damage via the ILK-PI3K/AKT pathway. Zool Res. 2023;44:620–35.
23. Yan L, Tu W, Zhao X, Wan H, Wu J, Zhao Y, et al. Stem cell transplantation extends the reproductive life span of naturally aging cynomolgus monkeys. Cell Discov. 2024;10:111.
24. Bahrehbar K, Gholami S, Nazari Z, Malakhond MK. Embryonic stem cells-derived mesenchymal stem cells do not differentiate into ovarian cells but improve ovarian function in POF mice. Biochem Biophys Res Commun. 2022;635:92–8.
25. Takashima Y, Era T, Nakao K, Kondo S, Kasuga M, Smith AG, et al. Neuroepithelial cells supply an initial transient wave of MSC differentiation. Cell. 2007;129:1377–88.
26. Liu JA, Cheung M. Neural crest stem cells and their potential therapeutic applications. Dev Biol. 2016;419:199–216.
27. Carrasco-Juan JL, González-Gómez M, Tapia O, García-Hernández S, Vega-Falcón A, Méndez-Medina R, et al. The origin of ovarian Leydig cells: a possibly solved enigma? Hum Cell. 2024;37:1544–52.
28. Li W, Huang L, Zeng J, Lin W, Li K, Sun J, et al. Characterization and transplantation of enteric neural crest cells from human induced pluripotent stem cells. Mol Psychiatry. 2018;23:499–508.
29. Zhou Y, Cai X, Zhang X, Dong Y, Pan X, Lai M, et al. Mesenchymal stem/stromal cells from human pluripotent stem cell-derived brain organoid enhance the ex vivo expansion and maintenance of hematopoietic stem/progenitor cells. Stem Cell Res Ther. 2024;15:68.
30. MacDonald BT, Tamai K, He X. Wnt/beta-catenin signaling: components, mechanisms, and diseases. Dev Cell. 2009;17:9–26.
31. Sonnen KF, Lauschke VM, Uraji J, Falk HJ, Petersen Y, Funk MC, et al. Modulation of phase shift between Wnt and Notch signaling oscillations controls mesoderm segmentation. Cell. 2018;172:1079–e9012.
32. Chambers SM, Fasano CA, Papapetrou EP, Tomishima M, Sadelain M, Studer L. Highly efficient neural conversion of human ES and iPS cells by dual Inhibition of SMAD signaling. Nat Biotechnol. 2009;27:275–80.
33. Liu H, Huang S, Wang W, Wang H, Huang W, Zhai Z, et al. Migration deficits of the neural crest caused by CXADR triplication in a human down syndrome stem cell model. Cell Death Dis. 2022;13:1018.
34. Yoshimatsu M, Ohnishi H, Zhao C, Hayashi Y, Kuwata F, Kaba S, et al. In vivo regeneration of rat laryngeal cartilage with mesenchymal stem cells derived from human induced pluripotent stem cells via neural crest cells. Stem Cell Res. 2021;52:102233.
35. Charney RM, Prasad MS, Juan-Sing C, Patel LJ, Hernandez JC, Wu J, et al. Mowat-Wilson syndrome factor ZEB2 controls early formation of human neural crest through BMP signaling modulation. Stem Cell Rep. 2023;18:2254–67.
36. Kamiya D, Takenaka-Ninagawa N, Motoike S, Kajiya M, Akaboshi T, Zhao C, et al. Induction of functional xeno-free MSCs from human iPSCs via a neural crest cell lineage. NPJ Regen Med. 2022;7:47.
37. Fukuta M, Nakai Y, Kirino K, Nakagawa M, Sekiguchi K, Nagata S, et al. Derivation of mesenchymal stromal cells from pluripotent stem cells through a neural crest lineage using small molecule compounds with defined media. PLoS ONE. 2014;9:e112291.

38. Scacheri PC, Tesar PJ. iPSC reprogramming is not just an open and shut case. Cell Stem Cell. 2017;21:711–2.
39. Kimbrel EA, Kouris NA, Yavanian GJ, Chu J, Qin Y, Chan A, et al. Mesenchymal stem cell population derived from human pluripotent stem cells displays potent Immunomodulatory and therapeutic properties. Stem Cells Dev. 2014;23:1611–24.
40. Zhang J, Chan Y-C, Ho JC-Y, Siu C-W, Lian Q, Tse H-F. Regulation of cell proliferation of human induced pluripotent stem cell-derived mesenchymal stem cells via ether-à-go-go 1 (hEAG1) potassium channel. American journal of physiology. Cell Physiol. 2012;303:C115–25.
41. Tian Z, Wang CK, Lin FL, Liu Q, Wang T, Sung TC, et al. Effect of extracellular matrix proteins on the differentiation of human pluripotent stem cells into mesenchymal stem cells. J Mater Chem B. 2022;10:5723–32.
42. Oja S, Komulainen P, Penttilä A, Nystedt J, Korhonen M. Automated image analysis detects aging in clinical-grade mesenchymal stromal cell cultures. Stem Cell Res Ther. 2018;9:6.
43. O'Hagan-Wong K, Nadeau S, Carrier-Leclerc A, Apablaza F, Hamdy R, Shum-Tim D, et al. Increased IL-6 secretion by aged human mesenchymal stromal cells disrupts hematopoietic stem and progenitor cells' homeostasis. Oncotarget. 2016;7:13285–96.
44. Herranz N, Gil J. Mechanisms and functions of cellular senescence. J Clin Invest. 2018;128:1238–46.
45. Zou T, Gao L, Zeng Y, Li Q, Li Y, Chen S, et al. Organoid-derived C-Kit(+)/SSEA4(-) human retinal progenitor cells promote a protective retinal microenvironment during transplantation in rodents. Nat Commun. 2019;10:1205.
46. Devine PJ, Perreault SD, Luderer U. Roles of reactive oxygen species and antioxidants in ovarian toxicity. Biol Reprod. 2012;86:27.
47. Banks CJ, Andersen JL. Mechanisms of SOD1 regulation by post-translational modifications. Redox Biol. 2019;26:101270.
48. Lu SC. Regulation of glutathione synthesis. Mol Aspects Med. 2009;30:42–59.
49. Eppig JJ, Reproduction. Oocytes call, granulosa cells connect. Curr Biol. 2018;28:R354–6.
50. Yin Y, Li H, Qin Y, Chen T, Zhang Z, Lu G, et al. Moxibustion mitigates mitochondrial dysfunction and NLRP3 inflammatory activation in cyclophosphamide-induced premature ovarian insufficiency rats. Life Sci. 2023;314:121283.
51. Chen Y, Zhao Y, Miao C, Yang L, Wang R, Chen B, et al. Quercetin alleviates cyclophosphamide-induced premature ovarian insufficiency in mice by reducing mitochondrial oxidative stress and pyroptosis in granulosa cells. J Ovarian Res. 2022;15:138.
52. Zhao YX, Chen SR, Su PP, Huang FH, Shi YC, Shi QY et al. Using Mesenchymal Stem Cells to Treat Female Infertility: An Update on Female Reproductive Diseases. Stem Cells Int. 2019;2019:9071720.
53. Ding C, Qian C, Hou S, Lu J, Zou Q, Li H, et al. Exosomal miRNA-320a is released from hAMSCs and regulates SIRT4 to prevent reactive oxygen species generation in POI. Mol Ther Nucleic Acids. 2020;21:37–50.
54. Zhang L, Ma Y, Xie X, Du C, Zhang Y, Qin S et al. Human pluripotent stem cell-Mesenchymal stem cell-Derived exosomes promote ovarian granulosa cell proliferation and attenuate cell apoptosis induced by cyclophosphamide in a POI-like mouse model. Molecules. 2023;28.

Publisher's note